Journal of Applied Physics

In situ surface acoustic wave field probing in microfluidic structures using optical transmission interferometry

Cite as: J. Appl. Phys. **129**, 244503 (2021); https://doi.org/10.1063/5.0055231
Submitted: 27 April 2021 • Accepted: 04 June 2021 • Published Online: 28 June 2021

R. Weser and H. Schmidt

Journal of Applied Physics ARTICLE scitation.org/journal/jap

In situ surface acoustic wave field probing in microfluidic structures using optical transmission interferometry

Cite as: J. Appl. Phys. **129**, 244503 (2021); doi: 10.1063/5.0055231
Submitted: 27 April 2021 · Accepted: 4 June 2021 ·
Published Online: 28 June 2021

R. Weser[a] and H. Schmidt

AFFILIATIONS

Leibniz Institute for Solid State and Materials Research Dresden, SAWLab Saxony, Helmholtzstr. 20, 01069 Dresden, Germany

[a]**Author to whom correspondence should be addressed:** r.weser@ifw-dresden.de

ABSTRACT

The generation of mechanical driving forces in fluids at the microscale can be efficiently realized using acoustic actuators. For this purpose, bulk or surface acoustic waves (SAWs) are typically excited by an electroacoustic transducer, and the acoustic energy is subsequently coupled to the fluid. The resultant acoustic pressure field in the fluid allows for precise manipulation of immersed objects and also for the agitation of the fluid itself. In general, the fluidic actuation capability is mainly determined by the mechanical displacement amplitude at the interface between the fluid and the acoustically active surface. In the case of SAW-based actuators, the fluid most often is directly attached to the substrate surface along which the surface waves propagate. Hence, the lateral distribution of surface displacement amplitude, i.e., the surface acoustic wave field, at the fluid–substrate interface is of particular interest in order to achieve full control of the fluidic actuation. Here, we present a reliable experimental method for the *in situ* determination of the SAW field on fluid loaded substrate surfaces based on laser interferometry. The optical accessibility of the fluid–substrate interface is realized via transmission through the anisotropic, piezoelectric substrate material requiring only an additional calibration procedure in order to compensate the parasitic influence of effects based on different indices of refraction as well as on complex acousto-optic effects. Finally, the proposed method is demonstrated to yield reliable results of displacement amplitude on the fluid loaded surface and thus, to provide a valuable insight into acoustofluidic coupling that was not available so far.

I. INTRODUCTION

Surface acoustic waves (SAWs) are able to efficiently induce driving forces in microfluidic devices in order to realize fluid streaming, manipulation of immersed particles or cells as well as the generation of fluid droplets.[1–7] For this purpose, Rayleigh type SAW are typically utilized due to their dominant out-of-plane component of displacement amplitude that basically induces the transfer of momentum from the substrate to the fluid.[8,9] Hence, the knowledge of the lateral distribution of displacement amplitude, i.e., the surface acoustic wave field, is mandatory for a well-founded understanding of acoustically induced forces in the fluid as well as for an appropriate design of SAW-based devices. The SAW field mainly is determined by the arrangement of interdigital transducers (IDTs) typically used to excite SAW on a piezoelectric substrate,[10] and also by the microfluidic structure, i.e., the fluid enclosed by a vessel both directly attached to the substrate surface. The physical presence of such a surface loading affects the propagation of SAW and changes displacement amplitude both in magnitude and phase, at which the attenuation of SAW due to a radiation of acoustic energy into the fluid or material of the vessel wall becomes clearly noticeable.[11] Most often, the SAW field in the presence of microfluidic structures (fluid-filled vessel) is determined by simulation based on semi-analytical or fully numerical approaches.[12–17] However, simulations are limited to comparably simple arrangements due to the complexity of models as well as to the required resolution of simulation. Moreover, elastic and electric properties of the involved materials need to be known very precisely, and an ideal interface between the substrate and surface loading with well-defined mechanical and electroacoustic coupling is assumed. Hence, a significant discrepancy between the model and the real device occurs if at least one of the assumptions is not completely fulfilled. In principle, this drawback can be overcome by

measuring the SAW field. Experimental determination of the lateral distribution of surface normal displacement amplitude using optical interferometry, more precisely laser Doppler vibrometry, was merely realized for SAW devices in the absence of surface loading, i.e., neither fluid nor vessel were present, in order to ensure direct optical accessibility of the vibrating surface.[10,18–21] Corresponding results allow for the clarification of principal SAW field characteristics, but do not provide further information about acoustofluidic interaction at the interface between the solid substrate surface and fluid (or other surface loading). Another approach based on laser Doppler vibrometry has been reported utilizing optical reflection at the surface of the fluid, i.e., at the interface between the fluid and ambient air, to experimentally study capillary waves in fluids driven by surface acoustic waves.[22] However, this method does not provide reliable results of surface displacement amplitude at the fluid–substrate interface.

Here, we present an optical measurement method based on a conventional laser Doppler vibrometer (LDV) setup with optical transmission through the substrate material that allows for the determination of the SAW displacement amplitude in the presence of surface loading, i.e., at the interface between substrate and microfluidic structure.[23] It is important to note that the SAW field measured in a transmission mode does not directly yield the real SAW amplitude because of the influence of optical transmission through the piezoelectric substrate material. In fact, the displacement amplitude evaluated from the Doppler shift appears to be higher due to piezoelectric, elasto-optic, and electro-optic effects evoking very complex changes of the effective optical path length and the local density inside the piezoelectric substrate. Moreover, in the case of anisotropic substrate materials, birefringence can occur, which causes a splitting of the incident laser beam due to different refractive indices for the ordinary as well as the extra-ordinary laser beam.[24,25] To overcome this problem, a linear polarizer is used to select one beam and to ensure precise laser focusing at a single point at the interface between the substrate and microfluidic structure. Finally, a calibration of LDV data captured this way is realized based on a correction coefficient for the SAW amplitude ratio derived from a direct comparison between standard and transmission measurement on the unloaded surface.

II. MEASUREMENT SETUP

The measurement of SAW displacement amplitude is exemplarily carried out for a SAW device based on a 128° rotated Y-cut of lithium niobate single crystal (128°Y $LiNbO_3$) typically utilized to realize SAW-driven microfluidics. Four interdigital transducers (IDTs) are arranged at the top side of the double side-polished substrate forming two pairs each with two opposing IDTs at a distance of 3.2 mm (Fig. 1). The corresponding SAW propagation directions are parallel to the X axis of the crystal and to the X + 90° direction, respectively. Both directions allow for the excitation of Rayleigh type SAW characterized by a dominant out-of-plane component of displacement amplitude. All IDTs exhibit the same aperture (1.2 mm), while the period as well as the number of electrode finger pairs are adapted for both orientations in order to achieve impedance matching at a common resonance frequency of 32.4 MHz.[10] IDT electrode metallization is realized using the conventional lift-off technique and deposition of subsequent layers of titanium (5 nm) and aluminum (295 nm) on the $LiNbO_3$ substrate. An additional passivation layer (500 nm SiO_2) is deposited on the complete structure in order to protect the electrodes from corrosion and to improve adhesion of the microfluidic vessel. The microfluidic vessel comprising inlet and outlet channels and a cavity with lateral dimensions 1.2 mm by 1.2 mm and a height of 200 μm is fabricated from polydimethylsiloxane (PDMS, Sylgard 184, Dow Corning) by mold-assisted casting and bonded to the top side of the substrate surface. The center of the vessel is aligned to the center between the four IDTs (Fig. 1). The complete SAW device is mounted and IDTs are electrically connected on a custom-built holder allowing for optical measurements from top [Fig. 2(a)] as well as from bottom side [Fig. 2(b)]. The inlets and outlets of the microfluidic vessel are connected to an external fluid reservoir via silicone tubes and the fluid flow is realized using a peristaltic pump (ISM 597, Ismatec).

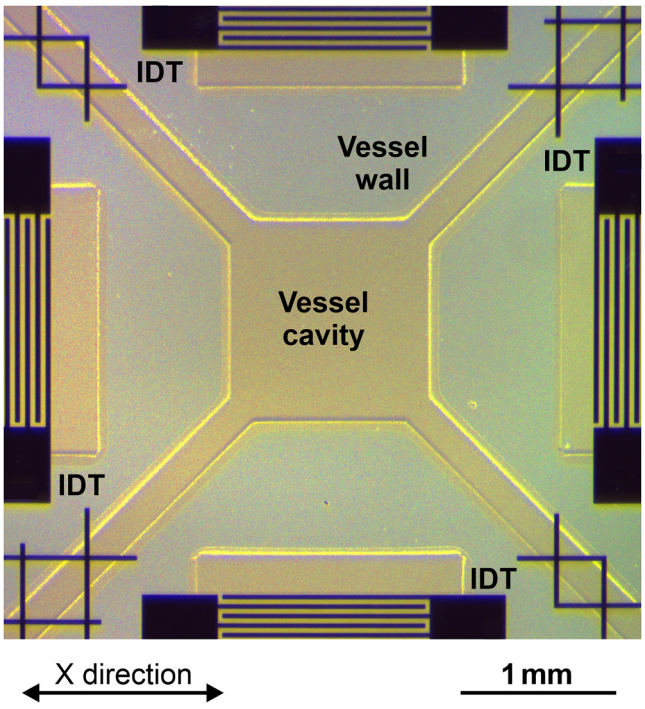

FIG. 1. Microphotograph of the center of the SAW device with the PDMS vessel attached to the substrate surface. Edges of the PDMS are highlighted due to increased light scattering. The active area of interdigital transducers (IDT) is free from PDMS to enable efficient SAW excitation. The four inlets/outlets at the corners of the vessel are used for fluid supply.

The SAW device is electrically characterized using a vector network analyzer (VNA, E5071C, Keysight Technologies). Measurements are realized for the unloaded substrate surface as well as in the presence of the PDMS vessel for both cases, empty and water-filled. The electric transmission coefficients are determined for pairs of opposing IDTs in both propagation directions allowing for direct comparison of unloaded and loaded substrate surface (see

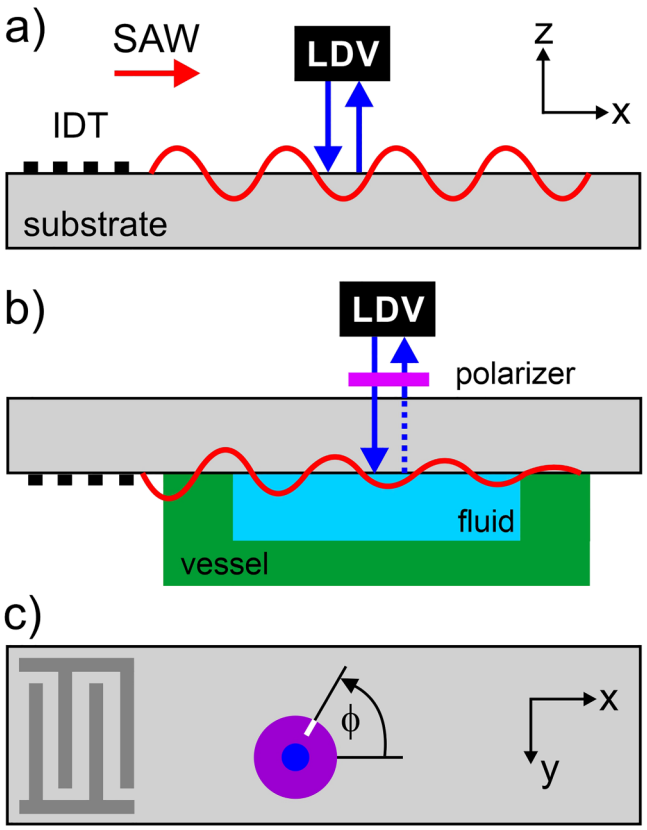

FIG. 2. Principle setup to measure surface acoustic wave (SAW) displacement amplitude using a laser Doppler vibrometer (LDV): (a) standard top side arrangement for the SAW device consisting of a piezoelectric substrate material and an interdigital transducer (IDT), (b) bottom side arrangement with the fluid-filled vessel and polarizer to suppress the second laser beam caused by a birefringent substrate material ($LiNbO_3$) during optical transmission, (c) top side view of (b) showing rotation angle of polarizer ϕ with respect to the orientation of the anisotropic substrate material during measurement.

Fig. S1 in the supplementary material). The out-of-plane component of SAW displacement amplitude is measured using an ultrahigh frequency laser Doppler vibrometer (LDV, UHF-120, Polytec) based on a heterodyne Mach-Zehnder interferometer.[26] This device emits a laser beam (measurement beam) that is focused to the surface under test. The spot size and the depth of focus can be adapted by using different microscopic objective lenses. For current measurements, an objective lens with a depth of focus equal to 1.6 μm was used in order to ensure precise focusing at the interface under investigation. The reflected measurement beam is interfered with a reference beam, and the modulation of optical phase (Doppler shift) is evaluated in order to determine the complex displacement amplitude of the surface under investigation. This measurement method relies on the assumption that the optical phase modulation is solely caused by the vibration of the surface under test, i.e., a time-dependent surface corrugation, and that there are no further changes of the effective optical path length (like a time-dependent change of the refractive index of the materials inside the optical path). This holds true for the characterization of SAW devices with bare (unloaded) surface [Fig. 2(a)], because the optical path length of the measurement beam is constant (apart from the surface displacement to be measured). In contrast to the unloaded surface scenario, SAW-based microfluidic actuators commonly contain a fluid volume most often surrounded by a vessel, both attached to the active surface (top side) of the piezoelectric substrate. The knowledge of the displacement amplitude at the substrate-fluid interface is of particular importance since it mainly determines the actuation capability of the SAW device. However, optical access for LDV measurements from the top side is barred since the presence of vessel and/or fluid causes distortion of the optical path of the LDV's measurement beam. In particular, bulk acoustic waves excited by the SAW and radiated into the vessel walls and into the fluid, evoke additional changes of the optical path length due to the presence of harmonic variations of the refractive index caused by the sound pressure via the elasto-optic effect.

An alternative approach is presented here based on optical transmission of the piezoelectric substrate material [bottom side measurement, Fig. 2(b)]. Single crystalline substrate material provides well-defined optical properties as compared to the vessel wall material and to the fluid, although the commonly used anisotropic lithium niobate shows birefringence. As a result, dependent on crystal orientation, the incident measurement beam is split into two parts propagating along slightly different optical paths (double refraction). A linear polarizer is inserted in the measurement beam allowing to separate both beams and to select one of them by suppressing the other. Thus, the orientation of the polarizer (rotation angle ϕ) needs to be appropriately chosen with respect to the crystal orientation of the $LiNbO_3$ [Fig. 2(c)]. Finally, the displacement amplitude measured in the transmission mode (from bottom side) needs to be corrected in order to achieve the real SAW amplitude at the top side.

III. CALIBRATION METHOD

The proposed calibration rests upon the direct comparison of the SAW field measured from top and bottom side for a SAW device with the unloaded surface (neither fluid nor vessel are present). Hereby, top side measurement corresponds to the usual measurement setup [standard LDV configuration, Fig. 2(a)], whereas the bottom side measurement is performed in the transmission mode through the crystalline substrate [Fig. 2(b)]. Figure 3 shows measured wave fields resulting from the superposition of surface acoustic waves excited by the arrangement of four IDTs. The result of standard top side LDV measurement [Fig. 3(a)] depicts characteristic distribution of SAW displacement amplitude showing periodic changes of minima and maxima. Highest amplitudes arise at the center ($|x| \leq 0.6$ mm and $|y| \leq 0.6$ mm) due to the superposition at the overlapping of the four SAW beams. The reduced amplitude around $y = 0$ results from SAW diffraction that arises in the X propagation direction at frequency 32.4 MHz due to limited aperture of the IDTs in combination with their comparatively small number of interdigital finger pairs, whereas this effect does not occur to the same degree in the X + 90° direction. Bottom side measurement is realized by rotating the sample by 180° around the crystal's X axis, because the LDV's laser beam needs to

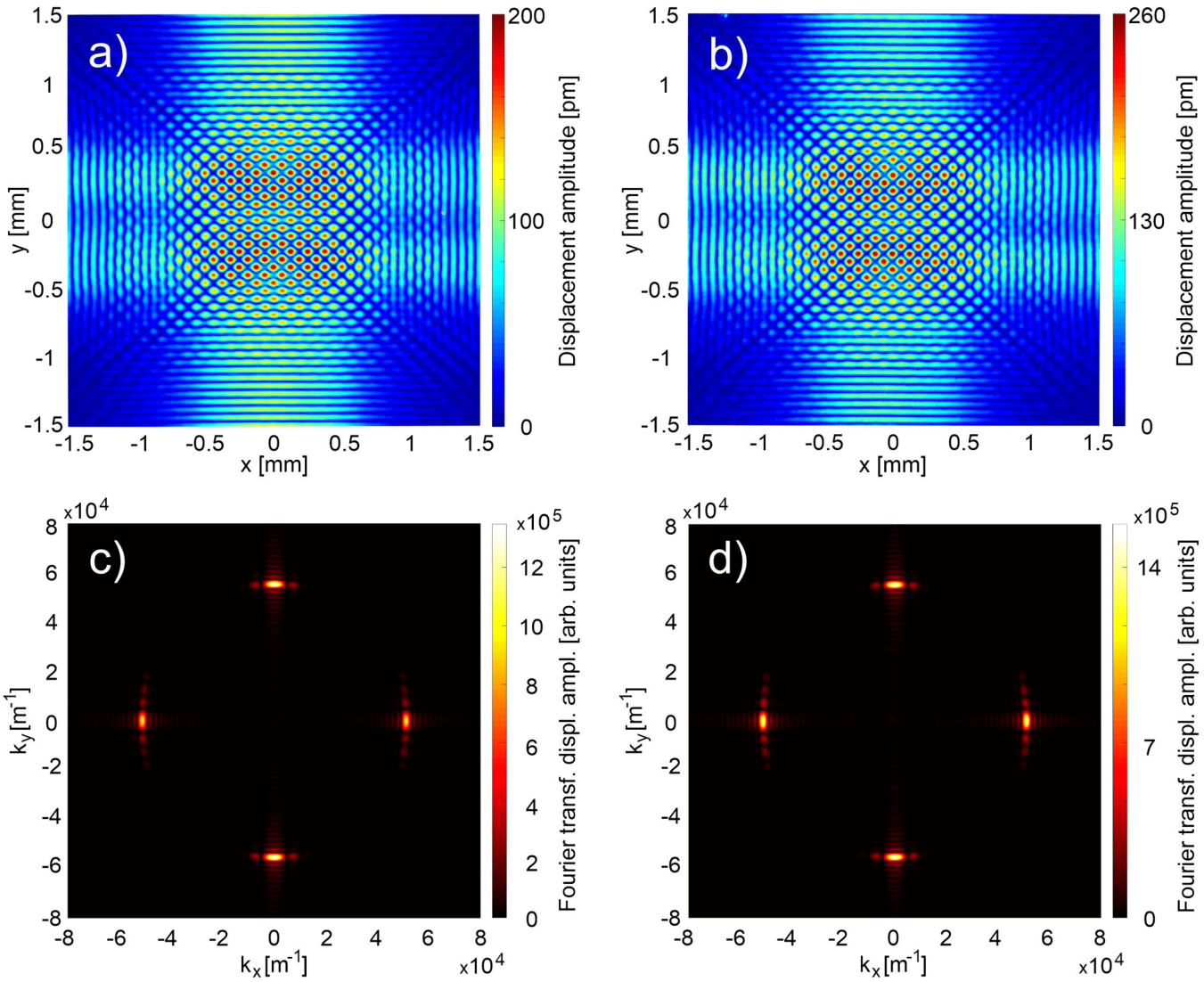

FIG. 3. Lateral distribution of surface normal displacement amplitude (magnitude) of two-dimensional standing surface acoustic wave field (2DsSAW) on unloaded surface measured at 32.4 MHz: (a) result of top side measurement, (b) uncorrected raw data from bottom side measurement (transmission with a polarizer oriented at $\phi = 0°$ with respect to crystal's X axis, i.e., parallel to the x-coordinate). The point of origin ($x = 0$, $y = 0$) is located at the center of the SAW device. The lateral resolution of LDV measurement is $\Delta x = \Delta y = 10\,\mu$m. The two-dimensional Fourier transform (magnitude) of both measurement results is plotted as a function of the wave vector $K = (k_x, k_y)$ for: (c) top side measurement (a) and (d) bottom side measurement (b).

hit the surface under test from above. The corresponding measurement result [Fig. 3(b)] shows qualitatively good agreement with the top side measurement [Fig. 3(a)]. Nevertheless, significant quantitative differences can be seen: The overall amplitude is higher, and the amplitude ratio of X and X + 90° direction is different. The latter relies on different relative orientations of the polarizer with respect to the crystal's axes and the optical anisotropy.

Higher amplitudes observed in the transmission mode can be attributed to additional changes of the optical path length originating from the influence of the refractive index of the crystal as well as from stress field distribution inside the substrate (penetration depth of the SAW). Hence, an overestimation of displacement amplitude at the top side of the substrate (focal plane) is observed when considering amplitude raw data from bottom side measurement. However, a calibration can be realized based on a spatial Fourier decomposition of measured wave fields in order to compensate differences mentioned before and to extract the real displacement amplitude at the top surface from bottom side measurement data.

The two-dimensional Fourier transform depicts similar results for top and bottom side measurement [Figs. 3(c) and 3(d)]. Four

maxima can be clearly identified, each corresponding to the travelling SAW (tSAW) excited by one of the IDTs. One pair of maxima is found at $k_x = 0$ and another one at $k_y = 0$. Each pair indicates two counter-propagating tSAWs of the same direction forming a standing SAW pattern in one dimension (1DsSAW), e.g., parallel to the X-propagation direction ($k_y = 0$). Superposition of both 1DsSAWs, with propagation directions perpendicular to each other, form a standing wave pattern in two lateral dimensions (2DsSAW). Line plots extracted from Figs. 3(c) and 3(d) for $k_x = 0$ and $k_y = 0$ allow for direct comparison between amplitudes extracted from top and bottom side measurement, respectively (Fig. 4). Maxima located at $k_y = 0$ arise at a wave number $|k_x| = 51\,474\ m^{-1}$ both for top and bottom side measurement corresponding to a SAW wavelength of 122 μm [Fig. 4(a)]. The corresponding amplitude ratio equals $c_X = 0.72$ and is used as correction coefficient for the X direction. Evaluation of maxima at $k_x = 0$ yields a wave number $|k_y| = 55\,201\ m^{-1}$ [Fig. 4(b), SAW wavelength: 114 μm] and an amplitude ratio of $c_{X+90°} = 0.89$ used as correction coefficient for X + 90° direction. The amplitude unbalance of counter-propagating tSAWs is approx. 1% for both directions (X and X + 90°) and does not affect the estimation of correction coefficients. See for direct comparison of corrected bottom side measurement and top side measurement (Fig. S2 in the supplementary material).

Figure 5 shows result of LDV bottom side measurement for the same SAW device but with loaded substrate surface, i.e., in the presence of fluid (water) and vessel (PDMS). The measured wave field reveals four SAW beams excited by the IDT arrangement [Fig. 5(a), raw data]. Significant attenuation of displacement amplitude can be observed caused by the leakage of acoustic energy into the PDMS and into the fluid. Correction coefficients extracted as described before for the case of the unloaded substrate surface facilitate the calibration of LDV measurement data in spatial frequency domain in order to determine the actual displacement amplitude at the substrate–fluid interface [Fig. 5(b)].

The proposed calibration method presupposes that reference measurements (top and bottom side on unloaded substrate surface) are performed for an equivalent SAW device as compared to the actual device with surface loading (fluid and/or vessel). In particular, the orientation of the crystal axes of the substrate with respect to the polarizer needs to be identical for bottom side measurements both with and without surface loading in order to accurately countervail the influence of birefringence of the anisotropic substrate material. This issue is not of importance for optically isotropic substrate materials. In general, comparable conditions needs to be ensured for reference and actual measurements, including identical optical properties of materials transmitted by the laser beam, namely the substrate (orientation and thickness) and the polarizer. Moreover, the twofold laser beam passage of the substrate and the polarizer during bottom side LDV measurement causes significant reduction of the light intensity. Together with reduced reflection at the substrate-fluid interface, the overall light intensity that can be detected by the photo diode of the LDV is much lower as compared to standard top side measurement. Nevertheless, reliable *in situ* LDV measurements of fluid loaded surfaces can be performed with only slight modification of the original optical setup.

IV. SAW PROPAGATION ON FLUID LOADED SURFACES

The presence of a fluid attached to the substrate surface affects the propagation of Rayleigh SAW due to relevant leakage of acoustic energy into the fluid (leaky Rayleigh wave). Leakage arises from the radiation of a longitudinal bulk acoustic wave into the fluid excited by the surface normal component of SAW displacement. Hence, a decrease of SAW amplitude u along coordinate x appears that is characterized by an exponential decay,

$$u(x) = \hat{u}\ \exp\left(-\frac{\alpha}{\lambda}x\right), \tag{1}$$

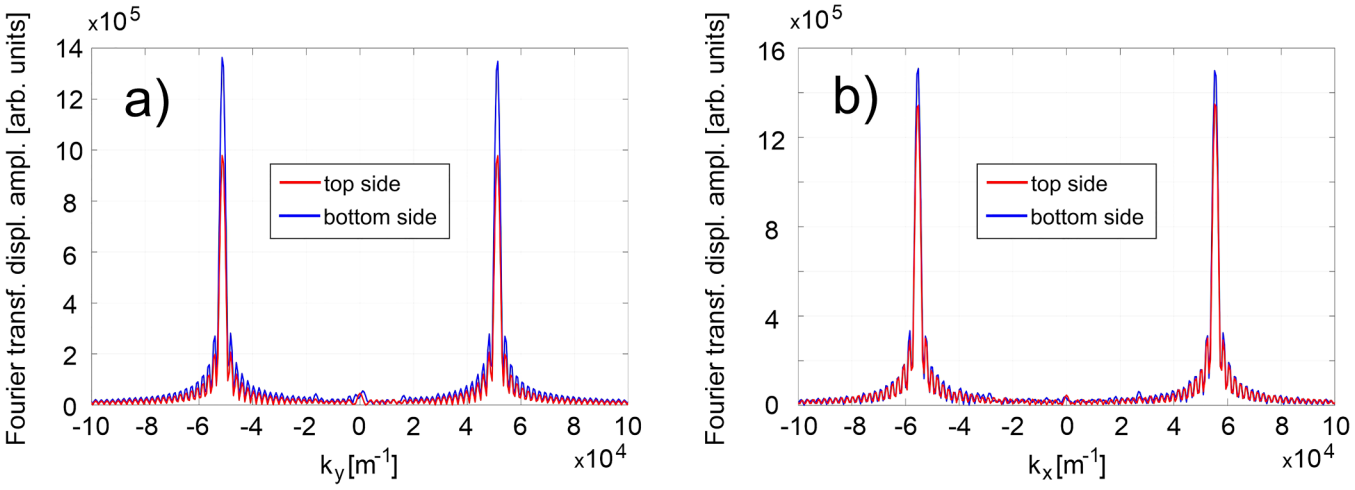

FIG. 4. Cross section of two-dimensional Fourier transform in Figs. 3(c) and 3(d) for top and bottom side measurement: (a) $k_y = 0$ (parallel to x and crystal's X direction), (b) $k_x = 0$ (parallel to y and X + 90° direction).

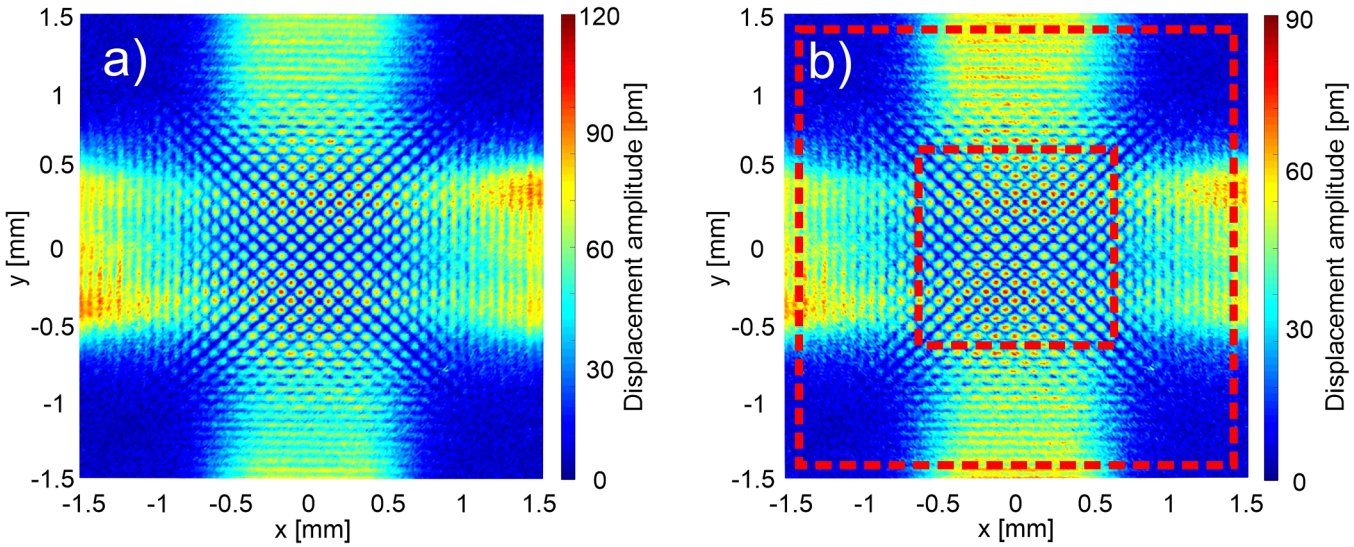

FIG. 5. Lateral distribution of surface normal displacement amplitude (magnitude) of 2DsSAW wave field on the substrate surface loaded with the water-filled PDMS vessel measured at 32.4 MHz: (a) raw data from bottom side measurement overestimating the amplitude (transmission with polarizer oriented at $\phi = 0°$ with respect to crystal's X axis, i.e., parallel to the x-coordinate), (b) corrected amplitude distribution using correction coefficients $c_X = 0.72$ and $c_{X+90°} = 0.89$. The lateral resolution of LDV measurement is $\Delta x = \Delta y = 10\,\mu$m. Squares (dashed red lines) indicate lateral dimensions of the fluid volume (1.2×1.2 mm^2, small box) and outer dimensions of the microfluidic vessel (2.8×2.8 mm^2, large box). The area between both boxes equals the width of the vessel walls (800 μm) firmly attached to the substrate surface (cf. Fig. 1).

with an attenuation coefficient roughly estimated by the ratio of acoustic impedances,[27,28]

$$\alpha = \frac{\rho_F v_F}{\rho_S v_{SAW}}, \tag{2}$$

where ρ_F and ρ_S refer to the density of the fluid and the substrate, respectively. The sound velocity of the longitudinal wave in the fluid equals v_F and v_{SAW} represents the phase velocity of the SAW. In this notation, the attenuation α corresponds to the decrease of SAW amplitude per SAW wavelength λ. The influence of shear-horizontal displacement amplitude of the SAW on the energy transfer is negligible because of the vanishing shear modulus of fluids. Besides, Rayleigh type SAWs are generally characterized by a minor shear-horizontal component.

The availability of laterally resolved measurement data for SAW displacement amplitude at the fluid loaded substrate surface facilitates the estimation of SAW attenuation based on experimental results. For this purpose, the amplitude of a traveling SAW (tSAW) is extracted from 2DsSAW [Fig. 5(b)] in spatial Fourier domain due to different wave vectors of tSAWs [cf. Figs. 3(c) and 3(d)]. Evaluation is exemplarily performed for both counter-propagating tSAWs in the X direction, both with and without fluid (water) inside the vessel (PDMS). Furthermore, the zero-order Fourier coefficient of the tSAW amplitude cross-sectional profile perpendicular to the propagation direction, i.e., calculated parallel to the y-coordinate, is evaluated to subsequently determine the amplitude as a function of propagation distance along the x-coordinate (Fig. 6).

Logarithmically scaled SAW amplitude depicts a linear decay if PDMS or water is attached to the substrate surface but remains almost constant if the vessel is empty, i.e., not filled with a fluid ($|x| < 0.6$ mm). Equivalent behavior for both counter-propagating tSAWs can be observed. Decay of displacement amplitude is obtained using linear interpolation. Measurement data of the empty vessel (PDMS, without water) are evaluated in the ranges of vessel walls ($-1.4\,\text{mm} < x \leq -0.6\,\text{mm}$ and $0.6\,\text{mm} < x \leq 1.4\,\text{mm}$) in order to

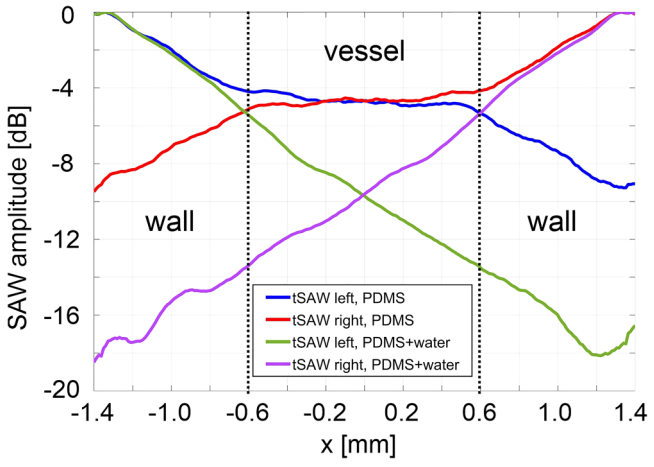

FIG. 6. Decay of SAW displacement amplitude (magnitude) caused by surface loading of the substrate surface. Amplitude of both counter-propagating traveling SAWs (tSAW) in the X direction is evaluated. The walls of the vessel (PDMS) are attached to the substrate at $-1.4\,\text{mm} < x < -0.6\,\text{mm}$ and at $0.6\,\text{mm} < x < 1.4$ mm; the fluid (water) is inside the vessel ($-0.6\,\text{mm} < x < 0.6$ mm, cf. Fig. 5).

TABLE I. Experimental results (decay of amplitude and insertion loss) evaluated at frequency 32.4 MHz are compared to the SAW attenuation calculated using Eq. (2). Insertion loss is determined from the difference of electrical transmission coefficients $|S_{21}|$ measured with VNA and divided by the nominal length of propagation paths of PDMS (1.6 mm) and water (1.2 mm). The decay of displacement amplitude is obtained from linear interpolation of logarithmically scaled SAW amplitude (Fig. 6) obtained from LDV measurements. In the case of PDMS, decay of SAW amplitude is separately determined for the first and the second wall of the vessel with respect to the particular tSAW propagation direction. In contrast, electrical transmission measurement provides the total insertion loss of both PDMS walls. SAW wavelength λ is estimated from measurement data of 2DsSAW with the fluid-filled vessel (cf. Fig. 5). Wavelength-normalized values are highlighted in gray.

		Experiment X direction, $\lambda = 121.7\,\mu$m			
		Decay of displacement amplitude (LDV)		Insertion loss (VNA)	
Material		tSAW left	tSAW right		Theory attenuation [Eq. (2)]
PDMS	1st wall	6.0 dB/mm	6.0 dB/mm	6.13 dB/mm	…
		0.73 dB/λ	0.73 dB/λ		
	2nd wall	5.5 dB/mm	5 dB/mm	0.745 dB/λ	0.496 dB/λ
		0.669 dB/λ	0.609 dB/λ		
Water		6.67 dB/mm	6.67 dB/mm	9 dB/mm	…
		0.811 dB/λ	0.811 dB/λ	1.095 dB/λ	0.703 dB/λ

determine the attenuation induced by the PDMS. Correspondingly, amplitude decay caused by the fluid (water) is determined from data of fluid filled vessel in the range of $-0.6\,\text{mm} < x \leq 0.6\,\text{mm}$. Experimental values are read in decibels per millimeter (dB/mm) and converted to dB/λ using the SAW wavelength λ (Table I). Corresponding results of the decay of SAW amplitude are given in Table I together with the insertion loss evaluated from electrical transmission measurement (see Fig. S1 in the supplementary material) as well as the attenuation calculated using Eq. (2) and material properties of $LiNbO_3$ ($\rho_S = 4640\,\text{kg/m}^3$,[29] $v_{SAW} = 3943$ m/s), PDMS ($\rho_F = 970\,\text{kg/m}^3$, $v_F = 1076$ m/s),[17] and water ($\rho_F = 998\,\text{kg/m}^3$, $v_F = 1483$ m/s).[30] PDMS is treated as a viscous fluid in this context, which seems to be reasonable due to the very low shear modulus.[29]

The decay of displacement amplitude on the water loaded surface yields accordant values for both counter-propagating tSAWs, which are lower than the insertion loss obtained from electrical transmission measurement. The reason for this seems to be incomplete bonding between the PDMS wall and the substrate, which is also indicated by amplitude profiles in Fig. 6 ($0.6\,\text{mm} < |x| < 0.8\,\text{mm}$). The resulting gap will be filled with water due to capillary forces. As a result, the effective attenuation length for the fluid is increased (>1.2 mm), which does not significantly influence the determination of relative amplitude decay from LDV data, whereas the insertion loss was divided by the nominal length of the fluid path (1.2 mm) yielding an overestimation of the normalized value. Relative insertion loss becomes more realistic if the effective attenuation length of the fluid (1.6 mm) is used. Thus, normalized insertion loss due to attenuation is rather 6.75 dB/mm or 0.821 dB/λ, which is in reasonable agreement with decay of displacement amplitude. However, experimental values are higher as compared to the theoretical value (0.7 dB/λ) calculated according to Eq. (2) for room temperature (20 °C) in any case. In fact, calculated attenuation might be slightly higher if moderate heating during LDV measurement is assumed (e.g., 0.72 dB/λ at 40 °C) due to the dissipation of acoustic energy (in water and PDMS) and localized heating induced by focused laser beam. Note also that the electric power applied to the SAW device is higher for LDV measurements (16 dBm) as compared to VNA measurements (0 dBm). However, significant increase of fluid temperature can be almost ruled out because heat will be discharged by the externally applied fluid flow.

The decay of displacement amplitude on the PDMS loaded surface depicts similar values for both counter-propagating tSAWs. However, relevant discrepancy is observed between the first and the second wall, with a lower decay for the second as compared to the first wall. Different attenuation for both walls is not plausible, in particular, because attenuation for the first wall should be equal to the attenuation for the second wall (and vice versa) in case of counter-propagating waves. Noticeably different values for the decay of displacement amplitude can be attributed to SAW diffraction effects. As a result, the cross sectional profile of the SAW beam varies with the distance to the IDT (cf. Figs. 3 and 5), which affects the determination of different decays of amplitude even if the attenuation is constant. A direct comparison with insertion loss indicates reasonable agreement for the first vessel wall. Following this, the decay of displacement amplitude seems to be underestimated for the second wall. In any case the attenuation calculated using Eq. (2) is significantly lower. The discrepancy between theoretical and experimental values is even higher for PDMS as compared to water and can be attributed to the rather rough estimation of attenuation [cf. Eq. (2)] as well as to uncertainty of effective material properties certainly differing from presumed values used for calculation. Moreover, treating PDMS as a viscous fluid neglects the shear modulus, even though it is quite low, and yields lower attenuation.

V. CONCLUSIONS

We have realized a reliable *in situ* measurement of surface normal displacement amplitude at the fluid–substrate interface of a SAW-based microfluidic actuator. A conventional laser Doppler vibrometer is used for this purpose together with an additional polarizer and the sample in optical transmission. The polarizer is inserted in the laser beam path in order to compensate the influence of birefringence of the anisotropic substrate material ($LiNbO_3$) that is transmitted by the laser beam to gain optical access to the fluid–substrate interface from the rear side of the substrate. A straightforward method for the calibration of acquired raw data is

proposed facilitating to counterbalance the overestimation of displacement amplitude due to refraction as well as to acousto-optic and electro-optic effects, which become relevant because of the optical transmission of the piezoelectric material. The proposed method is not limited to SAW-based devices but can be applied to all kinds of acoustically active surfaces as long as the interface under investigation is optically accessible. Thus, relevant optical reflection at the interface is required and the transmitted material needs to hold precise optical properties, including sufficient transparency, in order to ensure twofold transmission of the laser beam under well-defined conditions.

Finally, we successfully demonstrated the *in situ* observation of acoustic coupling into a microfluidic structure, which enables a more detailed inspection of acoustofluidic devices. In particular, relevant discrepancy was found between experimentally determined and calculated attenuation of SAW amplitude due to acoustic leakage into water and PDMS. However, experimentally determined distribution of displacement amplitude delivers valuable insight into device operation and can be used as input information for subsequent FEM simulations of microfluidic effects helping to provide more precise predictions of acoustofluidic actuation for real devices.

SUPPLEMENTARY MATERIAL

See the supplementary material for electrical characterization of the sample with unloaded and loaded substrate surface as well as for a direct comparison of displacement amplitude obtained from corrected transmission measurement with respect to reference measurement.

ACKNOWLEDGMENTS

The authors acknowledge the German Research Foundation (DFG Grant No. SCHM2365/17-1) for financial support.

DATA AVAILABILITY

The data that support the findings of this study are available within the article and its supplementary material.

REFERENCES

[1]T. Franke, A. R. Abate, D. A. Weitz, and A. Wixforth, "Surface acoustic wave (SAW) directed droplet flow in microfluidics for PDMS devices," Lab Chip **9**, 2625–2627 (2009).
[2]L. Y. Yeo and J. R. Friend, "Surface acoustic wave microfluidics," Annu. Rev. Fluid Mech. **46**, 379 (2014).
[3]X. Ding, P. Li, S.-C. S. Lin, Z. S. Stratton, N. Nama, F. Guo, D. Slotcavage, X. Mao, J. Shi, F. Costanzo, and T. J. Huang, "Surface acoustic wave microfluidics," Lab Chip **13**, 3626–3649 (2013).
[4]D. J. Collins, O. Manor, A. Winkler, H. Schmidt, J. R. Friend, and L. Y. Yeo, "Atomization of thin water films generated by high-frequency substrate wave vibrations," Phys. Rev. E **86**, 056312 (2012).
[5]M. Sesen, T. Alan, and A. Neild, "Microfluidic on-demand droplet merging using surface acoustic waves," Lab Chip **14**, 3325 (2014).
[6]D. J. Collins, B. L. Khoo, Z. Ma, A. Winkler, R. Weser, H. Schmidt, J. Han, and Y. Ai, "Selective particle and cell capture in a continuous flow using micro-vortex acoustic streaming," Lab Chip **17**, 1769–1777 (2017).
[7]A. Fakhfouri, C. Devendran, T. Albrecht, D. J. Collins, A. Winkler, H. Schmidt, and A. Neild, "Surface acoustic wave diffraction driven mechanisms in microfluidic systems," Lab Chip **18**, 2214–2224 (2018).
[8]A. D. Pierce, *Acoustics*, 3rd ed. (Springer, 2019).
[9]L. D. Landau and E. M. Lifshitz, *Fluid Mechanics*, 2nd ed. (Pergamon Press, 1987).
[10]R. Weser, A. Winkler, M. Weihnacht, S. Menzel, and H. Schmidt, "The complexity of surface acoustic wave fields used for microfluidic applications," Ultrasonics **106**, 106160 (2020).
[11]A. Winkler, R. Brünig, C. Faust, R. Weser, and H. Schmidt, "Towards efficient surface acoustic wave (SAW)-based microfluidic actuators," Sens. Actuators A **247**, 259 (2016).
[12]F. Guo, Z. Mao, Y. Chen, Z. Xie, J. P. Lata, P. Li, L. Ren, J. Liu, J. Yang, M. Dao, S. Suresh, and T. J. Huang, "Three-dimensional manipulation of single cells using surface acoustic waves," Proc. Natl. Acad. Sci. U.S.A. **113**, 1522 (2016).
[13]J.-C. Hsu and C.-L. Chao, "Full-wave modeling of micro-acoustofluidic devices driven by standing surface acoustic waves for microparticle acoustophoresis," J. Appl. Phys. **128**, 124502 (2020).
[14]N. R. Skov, P. Sehgal, B. J. Kirby, and H. Bruus, "Three-dimensional numerical modeling of surface-acoustic-wave devices: Acoustophoresis of micro- and nanoparticles including streaming," Phys. Rev. Appl. **12**, 044028 (2019).
[15]J. Guo, Y. Kang, and Y. Ai, "Radiation dominated acoustophoresis driven by surface acoustic waves," J. Colloid Interface Sci. **455**, 203 (2015).
[16]C. Devendran, T. Albrecht, J. Brenker, T. Alan, and A. Neild, "The importance of travelling wave components in standing surface acoustic wave (SSAW) systems," Lab Chip **16**, 3756 (2016).
[17]A. N. Darinskii, M. Weihnacht, and H. Schmidt, "Computation of the pressure field generated by surface acoustic waves in microchannels," Lab Chip **16**, 2701–2709 (2016).
[18]G. Greco, M. Agostini, I. Tonazzini, D. Sallemi, S. Barone, and M. Cecchini, "Surface-acoustic-wave (SAW)-driven device for dynamic cell cultures," Anal. Chem. **90**, 7450 (2018).
[19]C. Witte, J. Reboud, R. Wilson, J. M. Cooper, and S. L. Neale, "Microfluidic resonant cavities enable acoustophoresis on a disposable superstrate," Lab Chip **14**(21), 4277 (2014).
[20]R. Weser, A. N. Darinskii, M. Weihnacht, and H. Schmidt, "Experimental and numerical investigations of mechanical displacements in surface acoustic wave bounded beams," Ultrasonics **106**, 106077 (2020).
[21]R. W. Rambach, J. Taiber, C. M. L. Scheck, C. Meyer, J. Reboud, J. M. Cooper, and T. Franke, "Visualization of surface acoustic waves in thin liquid films," Nat. Sci. Rep. **6**, 21980 (2016).
[22]J. Friend and L. Yeo, "Using laser Doppler vibrometry to measure capillary surface waves on fluid-fluid interfaces," Biomicrofluidics **4**, 026501 (2010).
[23]F. Kiebert, S. Wege, J. Massing, J. König, C. Cierpka, R. Weser, and H. Schmidt, "3D measurement and simulation of surface acoustic wave driven fluid motion: A comparison," Lab Chip **17**, 2104 (2017).
[24]K. K. Wong, *Properties of Lithium Niobate* (INSPEC, 2002), EMIS Datareviews Series No. 28.
[25]R. S. Weis and T. K. Gaylord, "Lithium niobate: Summary of physical properties and crystal structure," Appl. Phys. A **37**, 191 (1985).
[26]C. Rembe, S. Boedecker, A. Dräbenstedt, F. Pudewills, and G. Siegmund, "Heterodyne laser-Doppler vibrometer with a slow-shear-mode Bragg cell for vibration measurements up to 1.2 GHz," Proc. SPIE **7098**,70980A (2008).
[27]R. M. Arzt, E. Salzmann, and K. Dransfeld, "Elastic surface waves in quartz at 316 MHz," Appl. Phys. Lett. **10**, 165 (1967).
[28]J. D. N. Cheeke, *Fundamentals and Applications of Ultrasonic Waves* (CRC Press, 2002).
[29]A. N. Darinskii, M. Weihnacht, and H. Schmidt, "Acoustomicrofluidic application of quasi-shear surface waves," Ultrasonics **78**, 10 (2017).
[30]L. Negadi, B. Feddal-Benabed, I. Bahadu, J. Saab, M. Zaoui-Djelloul-Daouadji, D. Ramjugernath, and A. Negadi, "Effect of temperature on density, sound velocity, and their derived properties for the binary systems glycerol with water or alcohols," J. Chem. Thermodyn. **109**, 124 (2017).